Simulation of Hole Shapes for Ultrashort Pulse Laser Percussion Drilling Processes

Philipp Bremer*[1], Joshua Farnschläder[1]

[1]*Fraunhofer Institute for Laser Technology ILT, Steinbachstr. 15 ,52074 Aachen, Germany*
**philipp.bremer@ilt.fraunhofer.de*

Micro-drilling with ultrashort laser pulses is becoming increasingly popular due to its productivity and precision. Applications such as water filtration and vibrating mesh nebulizers require micro-holes with an exit diameter of less than 5 µm and a high aspect ratio often greater than 10. At high aspect ratios multiple effects arise, that increase in complexity and for which an analytical explanation is not yet found. One of these effects, multi-reflection, remains particularly enigmatic. Although simulations for the shape of laser drilled holes do exist, they often fail to predict the geometries of micro-holes adequately. This paper presents an alternative approach for simulating ultrashort pulse laser micro drilling to enable accurate predictions of geometries. A model approach to address the multi-reflection effect is provided and the contribution of different effects on the generation of USP laser drilled holes are discussed.
DOI: 10.2961/jlmn.2026.02.2007
Keywords: laser drilling, micro-holes, percussion drilling, drilling of steel foil, simulation, ultra short pulsed

1. Introduction

Micro-holes, defined in this paper as holes with an exit diameter of less than 10 µm, play a crucial role in various applications, particularly in the fields of medicine and filtration technology. These small diameters when drilled through stainless steel foils up to 200 µm thick, lead to high aspect ratios greater than 10. At such high aspect ratios, phenomena such as multi-reflections of the laser radiation within the borehole become significant for the formation of the bore geometry. Although multi-reflection effects are recognized in literature, there is no complete analytical model yet. [1–3] Existing drilling simulations that predict the geometry of ultrashort pulse (USP) laser percussion drilling have been developed; however, they are not optimized for high aspect ratios and can only partially describe multi-reflection. Ray-tracing simulations have been known, however they are typically developed for nanosecond laser drilling, welding, or cutting applications. All of these processes are based on a melt dominant ablation and therefore the corresponding simulation not applicable to USP laser drilling. [1] The IFSW in Stuttgart has developed simulations for maximum drilling depths, where multi-reflection is linearly described with respect to the depth (z). [4,5] In this paper, a new simulation approach for USP percussion drilling in stainless steel foils is presented. It is designed to accurately simulate the created drill hole geometries. Several physical effects have been integrated into the simulation. The simulation allows for the activation and deactivation of these effects. This approach aims to enhance our understanding of the effects implications, as well as the relevance of various phenomena in shaping borehole geometry. The simulation will be calibrated and compared with experimental data to validate its accuracy and reliability

2. Physical principles and explanation of simulation

In this chapter, the relevant physical principles and effects used in the simulation are explained. The basis functionality of the simulation, which is based on calculating the projected fluence at the borehole wall is presented. Furthermore, the implementation of the various effects are described, like laser caustic, angle dependent absorption and multi-reflection.

2.1 Wall angle of drilling hole for given fluence

In USP laser ablation, the threshold fluence is used to define the minimum energy density required for material removal. For stainless steel, this threshold fluence is < 0.1 J/cm². A fluence below this value does not remove the material but rather heats or modifies the surface. When a laser beam strikes an inclined surface (in this case, the bore wall), the irradiated area becomes larger compared to the nominal area. Figure 1 schematically illustrates the larger irradiated area.

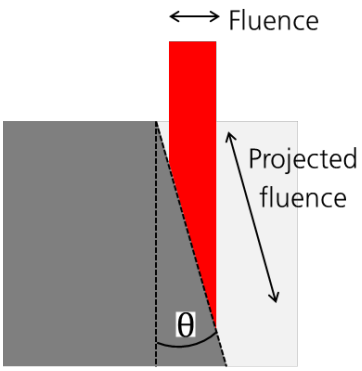

Fig. 1 definition of the wall angle θ and illustration of projected fluence.

In this paper, parameters or variables derived from the larger area are defined as "projected" variables. Thus, the projected focal area on the borehole surface is larger than the focal area in the focus of the laser caustic, and the projected fluence is smaller, as fluence is inversely proportional to the area. The minimum or final wall angle θ_{min}, for which no ablation would occur, is calculated using the fluence of the laser F(r) and the threshold fluence F_{th} according to Formula (1).

$$\theta_{min} = \arcsin\left(\frac{F_{th}}{F(r)}\right). \quad (1)$$

If the projected fluence falls below the threshold fluence of a material, the ablation process stops. [6] This relationship indicates the minimum wall angle that can be achieved with a given peak fluence and threshold fluence. Furthermore, this relationship holds true only if there is no heat accumulation and no melt-based ablation process during a USP laser drilling. The wall angle can be determined not only for a single value but continuously for a fluence distribution. The technical solution is a discretized fluence distribution and for each small increment the minimum wall angle is calculated. This yields the borehole shape for a given intensity distribution. Figure 2 displays the bore geometry for three different fluence distributions.

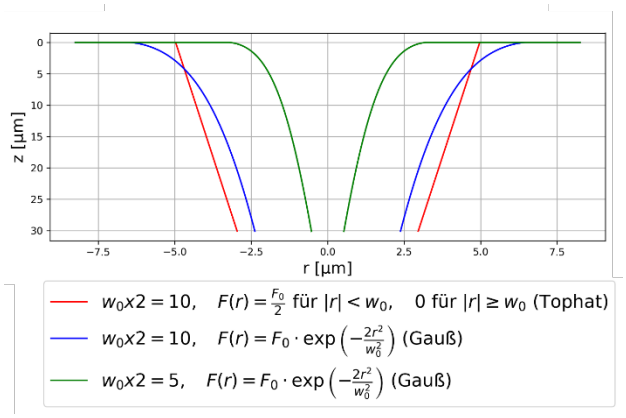

Fig. 2 Simulation of borehole geometry for different fluence distributions.

The red graph illustrates the simulated bore geometry for a specific fluence value, representing the case of a perfect top-hat profile, where the wall angle remains constant throughout the bore. The red and blue curves represent simulated bore geometries for fluence distributions with a perfect gaussian profile for different focal diameters. The bore profile exhibits the characteristic “trumpet” like shape of a USP percussion bore and does not maintain a constant wall angle. The simulation presented up to this point is referred to in the following sections of the paper as the simulation without additional effects or basic simulation. In the subsequent chapters, effects that upgrade this basic simulation will be discussed.

2.2 Angle dependent absorption

The absorption coefficient depends on the angle of incidence of light or laser radiation on the surface of the processing area. The angle dependent absorption is described by the Fresnel equations [7]. To calculate the formula, the material specific refractive index is required, which is reported in the literature to be approximately 1.9+i*3.5 for the given wavelength of 515 nm [8]. The absorption coefficient for steel calculated from this refractive index found in literature is depicted in Figure 3 in the blue curve.

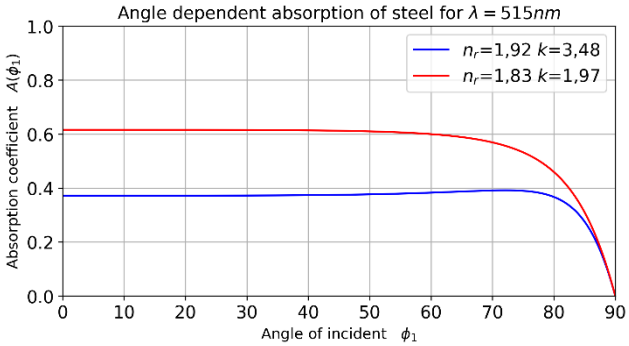

Fig. 3 Angle dependent absorption of stainless steel for 515 nm for two different refractive indexes.

For the implementation of the Fresnel equations in the simulation, the fluence value is multiplied by the absorption coefficient, depending on the local wall angle. The threshold fluence is multiplied by the initial absorption coefficient for a flat surface to obtain the absorbed threshold fluence. The absorbed threshold fluence is not angle dependent. Therefore, the absorbed fluence is normalized to the absorption coefficient for an angle of incidence equal to 0 degrees. The absolute value of the absorption coefficient is therefore not relevant, but the dependency of the angle of incident is.

The red curve in Figure 3 shows an absorption dependence that (as will be explained in a later part of this paper) is determined by a fit from the experimental data. Due to a significantly different value for the imaginary part of the refractive index, the initial absorption increases. However, the refractive index fluctuates significantly depending on the steel alloy used, so the literature value is only partially informative. In later parts of this paper the effect of the different refractive indexes on the simulation is discussed.

2.3 Divergent laser caustic

The influence of the beam caustic is also integrated into the simulation. For this purpose, the radius of the fluence distribution is defined as a function of z and calculated according to equation (3).

$$F(r,z) = F_0\, exp\,(\tfrac{-2r^2}{w(z)^2}). \quad (2)$$

$$w(z) = w_0\sqrt{1+(\tfrac{z}{z_r})^2}. \quad (3)$$

The implementation in the simulation occurs through an additional dependence of the fluence on z instead of only on r, as seen in equation (2).

2.4 Multi-reflection factor

To describe the multi-reflection in the borehole, there is no well-established physical model. Therefore, this paper presents an empirical model, that aims to describe the influence of multi-reflections by an increase of the local fluence. The fluence is multiplied by the multi-reflection factor, m, which is defined according to Formula (4).

$$m = \overset{\text{I}}{1} + \overset{\text{II}}{(1-\text{A})} * m_1 * \overset{\text{III}}{cos(\theta)^{m_2}} * \overset{\text{IV}}{\left(\frac{z}{r}\right)^{m_3}}. \quad (4)$$

For laser radiation irradiating a flat surface with an aspect ratio of 0, the multi-reflection factor is defined as 1, meaning it does not affect the fluence distribution by multiplication, thus necessitating term I. Factor II consists solely of the angle dependent reflection, or one minus the angle dependent absorption coefficient, as the intensity of all reflections in the borehole increases linearly with the reflection coefficient. However, not all reflections are reflected back into the borehole, depending on the hole geometry. Therefore, additional geometric terms must be introduced. A steeper bore wall ensures that reflections and scattering at the bore wall are more likely to be reflected back into the borehole, leading to the introduction of factor III. This also applies to a high aspect ratio. Factor IV specifies the local aspect ratio. High aspect ratios lead to more reflections and scattering in the borehole, suggesting that the effect of multi-reflection increases with the aspect ratio. Whether factors III and IV increase linearly is unknown, which is why parameters m2 to m3 are included. The parameters m1 to m3 are used to calibrate the multi-reflection factor, as the exact relationships between multi-reflection and borehole geometry are not yet fully understood. To calibrate the model, the parameters m1-m3 will be fitted to the experimental data collected in the experiments described in the following.

3. Conducted Experiments for Calibration

In this chapter, the calibration and validation of the simulation are performed. For this purpose, percussion drilling is conducted on stainless steel foils of various thicknesses, and the geometry is evaluated. Simulated exit diameters are compared with the measured exit diameters.

3.1 Experimental Setup and parameters

For the experiments, a USP laser from Trumpf is used. The beam source is from the TruMicro 2000 series and has a pulse duration of 900 fs, an average power of 75 W at 600 kHz, and a maximum pulse energy of 125 µJ. The wavelength is green at 515 nm. For the percussion drilling, a repetition rate of 0.6 kHz is consistently used, and the pulse energy, or fluence, is varied. This ensures a minimal thermal load to avoid thermal effects such as melting. Table 1 lists all the varied process parameters for the experiments.

Table 1 Varied process parameters for percussion drilling experiments.

Parameters	Values
Focus diameters [µm]	9.7,13.1,15.7
Steel foil thickness [µm]	25,50,75,150,200
Approx. Fluence values [J/cm²]	1,2,4,6,8,10,12,14,16,18, 20

The focal diameters listed in Table 1 is measured using an imaging system composed of a simple lens, a beam attenuator, and a camera from IDS. Using the lens, the focal diameter is projected onto the camera sensor with a known magnification, allowing for accurate determination of the focus size.

Table 2 Parameter of varied laser caustic.

Focal length [mm]	Focus diameter [µm] (measured)	Rayleigh length [µm] (calculated)
48	9.7	110
67	13.1	201
100	15.7	289

Combining all parameters in Table 1, 165 parameter sets are recorded, with each parameter set being executed three times to enable statistical analysis. Each exit diameter is measured using a optical microscope with both reflected and transmitted illumination. Figure 4 shows a measuring example.

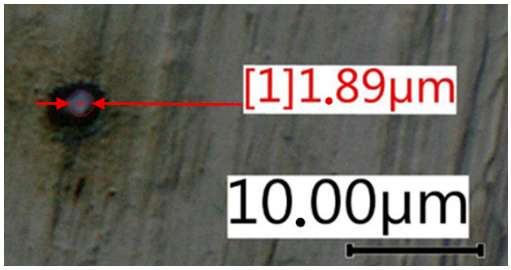

Fig. 4 Example measurement of exit diameter.

Due to the microscope's resolution, measuring hole exit diameters below 3 µm is challenging, and holes with diameters under 3 µm are not circular. Multiple holes within each parameter set are measured and the resulting variability is captured in the statistical uncertainty.

3.2 Calibration and fitting of the simulation

For the simulation, the multi-reflection factor must first be calibrated. For this purpose, the parameters m1 to m3 are fitted to all data points. The exact refractive index of the material for the wavelength used is not known. Only a refractive index for a similar steel was found in the literature (see chapter 2.2). Therefore, a new refractive index is determined by fitting the simulation to the data. The refractive index

provided by the literature, the refractive index determined by fitting, and the parameters m1 to m3 are listed in Table 3.

Table 3 Varied process parameters for percussion drilling experiments.

Parameters	Value
M1	0.105
M2	0.29
M3	0.98
Fitted refractive index	1.83 + i*1.97
Refractive index from literature	1.92+ i*3.48

3.3 Validation of the simulation

The exit diameters determined by the simulation can be compared with the experimentally determined exit diameters to assess the precision of the simulation. Furthermore, the effects discussed in chapter 2 can be turned on and off. This allows for conclusions to be drawn about how each effect influences the exit diameters. In Figure 5, the experimentally determined exit diameters are compared with the diameters obtained from the simulation for a foil thickness of 150 µm. The exit diameters are plotted against the fluences used.

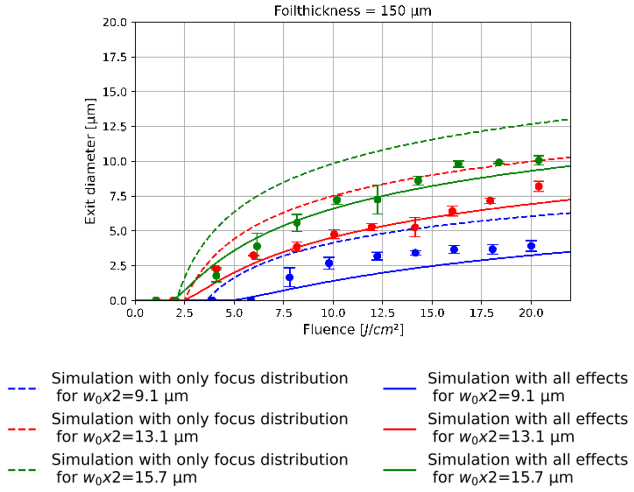

Fig. 5 Comparison between experimental results and simulation with and without additional effects.

The different colors represent the three focal diameters. The dashed line shows the results of the basic simulation, which is explained in section 2.1. In comparison, the solid line represents the final simulation with all implemented effects. As expected, the exit diameters increase with rising fluence. This is demonstrated by both the experimental data and the simulations. The basic simulation indicates exit diameters that are too large for all focus diameters, suggesting that additional effects beyond the fluence distribution in the focus are necessary to describe and understand the percussion drilling process.

4. Discussion

To make a more general assessment of the precision or quality of the simulation, the mean error or deviation for the various material thicknesses is determined. For different simulation settings, with various physical effects activated or deactivated, the difference between the simulated exit diameters and the measured exit diameters is calculated. In Figure 6, the simulation with the activated effect of angle-dependent absorption is shown as an example.

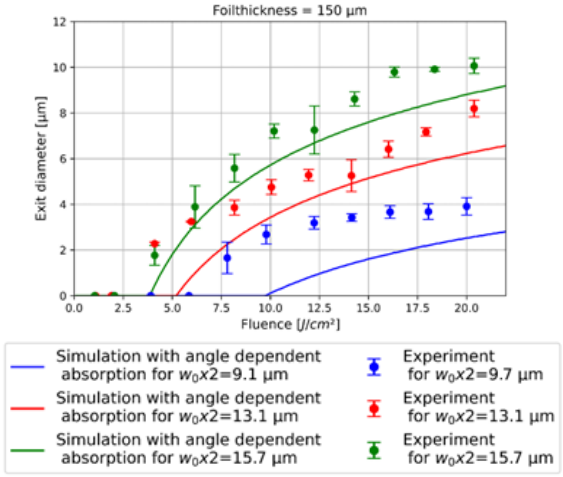

Fig. 6 Comparison between experimental results and simulation with implemented effect of angle dependent absorption; mean deviation of this graph is -1 ± 0.7 µm.

Taking the sum of the differences between simulated values and experimental values for all three focus diameters and calculating the average yields a total deviation of - 1 ± 0.7 µm for the graph in Figure 6.

When the mean deviation over the foil thickness is plotted for various simulation parameters, the graph in Figure 7 is obtained. The graph shows the deviation of simulations with different effects switched on over the foil thicknesses. A positive deviation means that the simulation predicts the exit diameter for the given foil thickness too large and a negative deviation means, the simulation predicts the exit diameter too small. The different markers show which refractive index is used for which simulation. For a circle shaped marker, the refractive index is irrelevant. A diamond shaped marker shows simulations using the refractive index found in literature. The square markers show simulations using the refractive index determined in this work by fitting. Figure 7 allows for an evaluation of how different effects contribute to the exit diameter. Furthermore, the graph shows the behavior of the effects for different foil thicknesses and thus different aspect ratios. In principle a higher foil thickness leads to higher aspect ratios and thus to complicated behavior in the drilling hole.

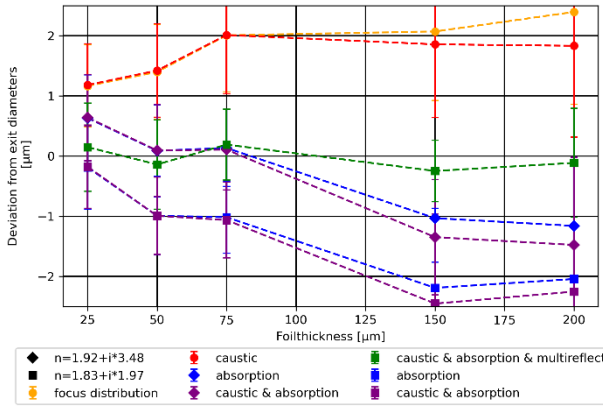

Fig. 7 Mean deviation of the simulated exit diameter from the measured exit diameter for different foil thicknesses and different effect switched on for the simulation.

The yellow curve represents the basic function from chapter 2.1 considering just the fluence distribution. A significant deviation with overly large exit diameters for all foil thicknesses is noticeable. In this simulation option the fluence distribution does not change at all with deeper drilling holes and therefore simulates the ablation in every depth z like it is in the focus plane. This results in exit diameters too large. The deviation increases with higher foil thicknesses, because for higher aspect ratios other effects become increasingly relevant. A pure consideration of the fluence distribution in the focus is therefore insufficient and effects are needed, that decrease the absorbed energy in deeper drilling depth and therefore lead to smaller exit diameters.

A logical next step to decrease the fluence with increasing depth z would be the implementation of the divergence of the radiation in the borehole. Since the peak fluence decreases in the deeper regions of the borehole due to the beam caustic, a smaller exit diameter is expected when the divergence is activated. This is represented by the red curve, which incorporates only the caustic. For small foil thicknesses, the caustic shows no noticeable difference. This is expected, as foil thicknesses below 100 µm are often smaller than the Rayleigh length. The Rayleigh length for the smallest focus is approximately 110 µm. For thicker foil thicknesses, it is observed that the red curve corrects the error downward and shows slightly better values. However, this correction is not significantly changing the exit diameter and cannot explain the smaller exit diameters compared to the simulated diameters.

A further logical step is the implementation of angle dependent absorption. This effect is examined in the blue curves alone and in the violet curves together with the effect of the caustic. The exit diameters are simulated to be smaller compared to the red and yellow curves. This is because even at the smallest foil thicknesses considered here (25 µm), aspect ratios exceeding 2 occur, resulting in an angle of incidence on the order of or above 80°. This leads to a significant decrease in absorption and therefore smaller exit diameters in the simulation. The effect is amplified with thicker foils, as the wall angle is steeper for high aspect ratios, resulting in a falling blue and violet curve.

For the refractive index from the literature, represented by the diamond-shaped markers, the absorption coefficient decreases later at higher angles of incidence (see comparison in Figure 3), leading to larger simulated exit diameters than for the refractive index determined in this work. Moreover, a local maximum of the overall absorption coefficient is observed at the Brewster angle. This local maximum could explain why, for a film thickness of 25 µm, the simulated exit diameters are even simulated too large for the diamond markers. However, because of statistical uncertainties, this connection cannot be established with confidence. For the refractive index fitted in this work (represented by the square markers), all exit diameters are simulated too small, especially for higher foil thicknesses.

Therefore, an effect is needed, which increases the absorbed energy or fluence mainly for high aspect ratios. The multi-reflection effect, which is introduced in the green curve, serves this problem. For the simulation option including the multi-reflection factor, the in this paper fitted refractive index (represented with square markers in Figure 7) is used. As a result, the exit diameter is sufficiently well described within the uncertainties across all foil thicknesses. As a note: This is not surprising, but designed to be that way, because of the fitting, that has been done to the parameters m1 to m3. Important is, that the multi-reflection factor contributes in a way, that the energy deposition for large foil thicknesses/ high aspect ratios increases in contrast to the last two effects. The multi-reflection factor m accounts for the reflected fluence portion that increases with the angle of incidence, rather than simply discarding it. Terms such as the aspect ratio z/r and the wall angle cos(θ) can consider the dependence of the borehole geometry on the portion of radiation that is reflected or scattered out of the borehole. This enables relatively precise statements about the geometry of the borehole, specifically regarding the exit diameter, even when classical models of USP processing are insufficient.

5. Conclusion and Summary

This paper presents a simulation for the prediction of exit diameters of USP laser percussion drilling in stainless steel foils. The simulation is based on the analysis of the fluence in the borehole and the calculation of the wall angle at which the fluence on the enlarged projected area of the tilted borehole wall is smaller than the threshold fluence. Based on these calculations, the geometry of the borehole can be simulated. Additionally, various effects that alter the fluence distribution in the borehole and thus influence the geometry are implemented in the simulation. The two already known effects are the divergence of the laser caustic in the borehole and the angle dependent absorption of the laser radiation on the tilted borehole wall. A simulation using only these effects is insufficient to accurately describe the exit diameters for large aspect ratios, as it predicts exit diameters that are too small. To correct this, multi-reflection or scattering in the borehole must be considered, as the reflected or scattered portion of the laser radiation is not completely reflected out of the borehole after initial interaction with the material. In this paper, an empirical model is presented for this effect in the form of the multi-reflection factor m. This factor accounts for the reflected portion of the laser radiation and depends on geometric parameters such as the local aspect ratio and the local wall angle. These geometric parameters are necessary because, for example, at higher aspect ratios of a borehole, the laser radiation is more easily reflected back and forth within the borehole due to a beam trapping effect.

By introducing this factor, it becomes possible to predict the exit diameters of micro-holes with higher aspect ratios more accurately and to understand the potential dependence of multireflection on the geometry of the borehole.

6. References

[1] M. F. Modest, Journal of Heat Transfer **128**, (2006), 653.
[2] K.-W. Park and S.-J. Na, Applied Surface Science **256**, (2010), 2392.
[3] A. Feuer, R. Weber, R. Feuer, D. Brinkmeier, and T. Graf, Appl Phys A **127**, (2021), 665.
[4] D. J. Förster, R. Weber, D. Holder, and T. Graf, Optics express **26**, (2018), 11546.
[5] D. Holder, R. Weber, T. Graf, V. Onuseit, D. Brinkmeier, D. J. Förster, and A. Feuer, Appl Phys A **127**, (2021), 943.
[6] D. Haasler, Tiefbohren in Metallen mittels ultrakurzen Laserpulsen. *Deep drilling in metals by means of ultra-short laser pulses*, 1. Auflage (Apprimus Verlag, Aachen, 2022),86.
[7] R. Poprawe, K. Boucke, and D. Hoffman, Tailored Light 1 (Springer Berlin Heidelberg, Berlin, Heidelberg, 2018), 68.
[8] B. Karlsson and C. G. Ribbing, Journal of Applied Physics **53**, (1982), 6340.

(Received: July 11, 2025, Accepted: April 21, 2026)